RESEARCH ARTICLE

Comparison of annulus fibrosus cell collagen remodeling rates in a microtissue system

Isabel N. Tromp[1] | Jasper Foolen[2] | Marina van Doeselaar[2] | Ying Zhang[3] |
Danny Chan[3] | Moyo C. Kruyt[1] | Laura B. Creemers[1] | Rene M. Castelein[1] |
Keita Ito[1,2]

[1]Department of Orthopaedic Surgery, University Medical Center Utrecht, Utrecht, The Netherlands

[2]Orthopaedic Biomechanics, Department of Biomedical Engineering, Eindhoven University of Technology, Eindhoven, The Netherlands

[3]School of Biomedical Sciences, Faculty of Medicine, The University of Hong Kong, Hong Kong SAR, China

Correspondence
Keita Ito, Department of Orthopaedic Surgery, G05.228, University Medical Center Utrecht, P.O. Box 85500, 3508 GA Utrecht, The Netherlands.
Email: k.ito@umcutrecht.nl

Funding information
Dutch Arthritis Foundation, Grant/Award Number: LLP12; EUROSPINE: 10-2017; Stryker Spine Research Grant; Fondation Yves Cotrel; Hong Kong Research Grants Council, Grant/Award Number: 17126319

Abstract

It has been suggested that curvature progression in adolescent idiopathic scoliosis occurs through irreversible changes in the intervertebral discs. Strains of mice have been identified who differ in their disc wedging response upon extended asymmetrical compression. Annulus fibrosus (AF) tissue remodeling could contribute to the faster disc wedging progression previously observed in these mice. Differences in collagen remodeling capacity of AF cells between these in-bred mice strains were compared using an in vitro microtissue system. AF cells of 8–10-week-old LG/J ("fast-healing") and C57BL/6J ("normal healing") mice were embedded in a microtissue platform and cultured for 48 h. Hereafter, tissues were partially released and cultured for another 96 h. Microtissue surface area and waistcoat contraction, collagen orientation, and collagen content were measured. After 96 h postrelease, microtissues with AF cells of LG/J mice showed more surface area contraction ($p < .001$) and waistcoat contraction ($p = .002$) than C57BL/6J microtissues. Collagen orientation did not differ at 24 h after partial release. However, at 96 h, collagen in the microtissues from LG/J AF cells was aligned more than in those from C57BL/6J mice ($p < .001$). Collagen content did not differ between microtissues at 96 h. AF cells of inbred LG/J mice were better able to remodel and realign their collagen fibers than those from C57BL/6J mice. The remodeling of AF tissue could be contributing to the faster disc wedging progression observed in LG/J mice.

KEYWORDS
annulus fibrosus, collagen, intervertebral disc, matrix remodeling, scoliosis

1 | INTRODUCTION

Adolescent idiopathic scoliosis (AIS) is a three-dimensional deformity of the spine and trunk that primarily affects previously healthy children and may seriously affect the quality of life.[1] Current treatment for scoliosis consists of intensive bracing for many years. The aim of bracing is to halt curve progression and prevent a large curvature that requires surgical treatment. However, the tendency of a curve to progress appears to be very difficult to predict as about 50% of the patients will not develop a severe curve even without

bracing. The reason for this difference in curve behavior is likely the consequence of individual adaptive mechanisms. Unfortunately, many efforts including genetic testing have failed to identify those patients who would benefit from bracing treatment.[2] Leaving us unable to distinguish between patients with a slow or fast progressing scoliotic curvature.

Already early in curve progression, it has been observed that the intervertebral disc (IVD) becomes deformed.[3] In fact, by investigating the individual contribution of the IVDs and the vertebral bodies, it was shown that AIS curves were characterized by a much greater deformation of the IVDs than the vertebral bodies.[4] These findings indicate that the IVDs are an important factor in the onset and progression of scoliosis. Since the disc does not become deformed by a growth process like bone but seems to undergo deformation via tissue production and/or remodeling, the matrix content and structural characteristics of the IVD are most likely the characteristic factors of the deformation process.

In the IVD of healthy adolescents, an organized network of abundant elastic fibers is found. However, in the scoliotic IVD, they become disrupted and sparse.[5] Additionally, scoliotic IVDs removed in the course of surgery showed distinct differences in biochemical and structural parameters compared to healthy IVDs, including an altered proteoglycan and collagen content and organization. Also, differences between the concave and the convex side have been noted, especially with respect to annulus fibrosus (AF) tissue fibers. Relative to the concave side, the collagen type I content of the convex side is increased with more cross-linking, indicating a higher collagen production, maturation, and stiffness.[6–8] Recently, shear wave elastography of the mechanical properties of the IVD confirmed that scoliotic IVDs may have stiffer AF in comparison to healthy controls.[9] This suggests that irreversible changes in the IVD, in particular the AF, may support or enhance scoliosis curve progression.

Recently, a reproducible mouse model of disc degeneration by looping the tail[10] was adapted to study disc wedging, that is, deformation. Using in-bred strains of mice with differences in their connective tissue healing capacity, that is, C57BL/6J, "normal healers" and MRL/MpJ, "fast healers,"[11] it was determined whether these mice would also differ in their disc wedging characteristics. They found that after 4 weeks of looping and 8 weeks of unlooping, MRL IVDs showed more AF recovery than those of the C57BL/6J mice, in terms of AF lamellar reorganization and maintenance of the IVD height. However, when the tails were looped for 8 weeks, and unlooped up to 16 weeks, C57BL/6J mice demonstrated better AF repair than in the MRL mice. This unexpected result could be consistent with the fact that MRL mice are able to more quickly and extensively remodel their AF tissue.[12] Thus, implying that the IVD deformation in MRL mice had become so extensive that it was not possible for them to recover thereafter.

We hypothesize that the difference between adolescents whose spines are predisposed to decompensate into persistent and progressive deformity and those spines of adolescents who will recover to physiologic curvature by the end of the growth spurt is caused by individual differences in AF collagen network adaptation in the early stages of development of spinal deformity. Furthermore, the rate of this adaptation would indicate the rate of curve progression. Hence, potential curve progression differences could be distinguishable by measuring collagen network adaptation potential of an individual's AF cells. As an initial exploration of this hypothesis, the goal of this study was to determine whether AF cells of in-bred LG/J (even better healers than MRL)[11] and C57BL/6J mice (normal healers) strains show a difference in collagen remodeling capacity in an in vitro microtissue assay system.

2 | MATERIALS AND METHODS

2.1 | Animals

LG/J and C57BL/6J mice were obtained from the Jackson Laboratory (USA) and kept in a Minimal Disease Area of the institutional Laboratory Animal Unit, a member of the Association for Assessment and Accreditation of Laboratory Animal Care International (AAALAC). The institutional animal ethics committee of the University of Hong Kong approved the studies (CULATR 3956-16).[13]

2.2 | Cell isolation and culture

A total of 14 (7 of each strain) 8–10-week-old mice were killed by cervical dislocation. The tails were soaked in 70% ethanol and cut open along the length. The AF were dissected aseptically from the tail under a stereo microscope. Approximately eight coccygeal AF from each tail were dissected and pooled together per mouse. Using a mixture of 0.0125% collagenase P (11213857001; Roche), 0.4% hyaluronidase (H3884; Sigma-Aldrich) and 0.1% elastase (LS002292; Worthington Biochemical) in HBSS (14175-079; Gibco), AF cells were isolated by digestion for 1.5 h at 37°C in an Eppendorf thermomixer at a shaking speed of 500 rpm. Digestion was stopped by adding 10 ml Dulbecco's modified Eagle medium with L-glutamine (DMEM; 12100-046; Gibco), supplemented by 2% fetal bovine serum (FBS; 10270106; Thermo Fisher Scientific) and 1% penicillin/streptomycin (15140122; Gibco). The mixture was passed through 70 µm cell strainer and spun down at 180 g for 10 min at room temperature. Hereafter the cells were cultured until passage 3 using culture medium containing DMEM (12100-046; Gibco), supplemented with 2.5% NaHCO3 (27778.293; NORMAPUR), 2% Na Pyruvate (P2256; Sigma-Aldrich), 2% HEPES (H-4034; Sigma-Aldrich), 10% FBS (10270106; Thermo Fisher Scientific), and 1% penicillin/streptomycin (15140122; Gibco). Additionally, Amphotericin B (Fungizone) (15290018; Gibco) was added to all cultures up to P1. Expansion of AF cells of LG/J mice, ultimately, resulted in a higher cell count compared to the AF cells of C57BL/6J mice, under equal culture conditions, suggesting that the proliferation rate of AF cells of LG/J mice was higher.

2.3 | Microtissue platform

Fabrication of the microtissue platform was performed according to the protocol by Foolen et al.[14] The microtissue platform was comprised of 10 constraining posts in a hexagon shape. As preparation, the microtissue platforms were sterilized by immersion in 70% ethanol overnight, and the wells were treated with 0.2% Pluronic F-127 (P2443; Sigma-Aldrich) in Milli-Q to impair cell adhesion. Hereafter, they were treated for 30 min with UV radiation. Cell-populated reconstituted collagen matrix tissues were produced by allowing them to anchor around the constraining posts. A gel mixture of growth medium, collagen type I (rat tail) (5056; Advanced Biomatrix) and 1 M NaOH, to neutralize the acidic collagen solution, was made with a final collagen concentration of 1.0 mg/ml. Cells were mixed with the gel at 2.5 million cells/ml gel. The cell–gel mixture was subsequently added to the system and left to gel for 45 min, after which warm growth medium was added to each well (4 ml, culture medium with 0.25 mg/ml L-ascorbic acid 2-phosphate sesquimagnesium salt hydrate (A8960; Sigma-Aldrich)) and cultured for 48 h. From an initial setup of 10 posts (unperturbed and isotropic) remodeling toward a six posts setup (perturbed and anisotropic) was induced by detaching the tissue over the perpendicular posts at 48 h after the start of culturing using forceps (Figure 1). Microtissues were further cultured for another 96 h. Posts were mounted on rigid substrates, and deflection of posts upon tissue contraction was not observed. During the culture period of 48 h and an additional 96 h postrelease, some tissues were lost due to being pulled off the posts by the cell-generated forces. Only those tissues that remained anchored to all 10 posts, or 6 posts after postrelease, were used for analysis of data.

2.4 | Tissue contraction

### 2.4.1 | Surface area and waistcoat contraction

Microtissue postrelease causes an alteration in support of the microtissue and the cells are stimulated to remodel the collagen in the microtissue from an isotropic (unaligned) to anisotropic
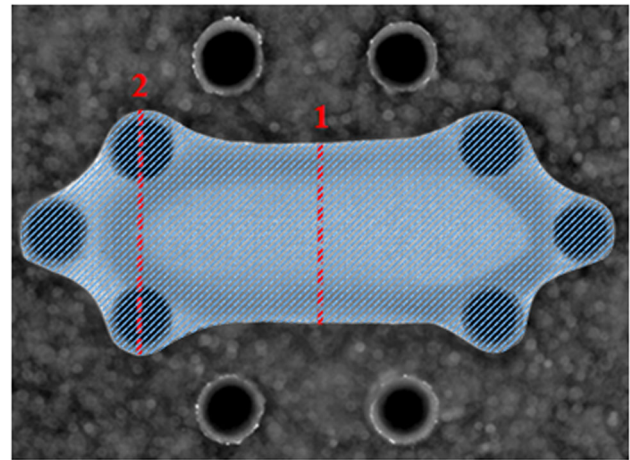
FIGURE 2 Microtissue surface area was analysed by measuring the whole surface area perpendicular to the posts (cross-hatched area) and waistcoat contraction was measured dividing minimum width (1)/maximum width (2) [Color figure can be viewed at wileyonlinelibrary.com]

(aligned) organization. This remodeling is also associated with tissue contraction where surface area and the "waistcoat" of the tissue with respect to the original surface/width provides a measure of collagen remodeling.

Digital top-down images of the tissue remodeling platform were made at different time points using a bright field microscope (MZ10F; Leica), connected to a CCD camera (DFC310FX; Leica) and quantified with digital image software (Application Suite 4.9.4, Leica). Microtissue surface area was analysed by contouring the tissue border of top-view images, and microtissue waistcoat contraction (minimum width/max post width across anchorage microposts) was quantified at the different time points. Both parameters were assessed using image analysis application Fiji[15] (Figure 2). A total of $N = 4$ nonpooled LG/J and $N = 2$ pooled LG/J tissues were used for analyses of surface area and waistcoat contraction. For C57BL/6J, a total of $N = 2$ nonpooled tissues and $N = 2$ pooled tissues were used for analyses. Tissues of nonpooled cells were made for both LG/J and
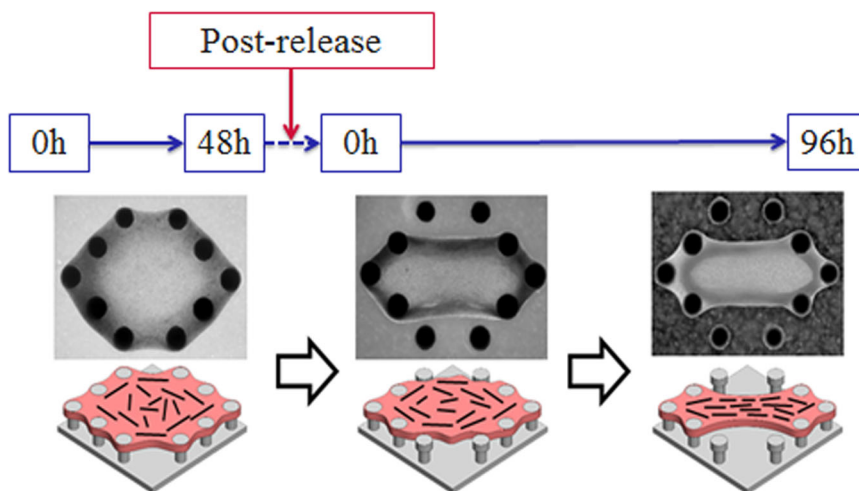
FIGURE 1 Representative images of microtissues remodeling in a dedicated platform from unperturbed and isotropic to perturbed and anisotropic after detaching the tissue with forceps after 48 h in culture [Color figure can be viewed at wileyonlinelibrary.com]

C57BL/6J in replicates. Pooling of extra cells was necessary because expansion of cells from some donors was insufficient to achieve the necessary number of cells. For replicates from the same donor, an average value was calculated and used as $N = 1$ for analyses.

2.5 | Collagen orientation

Microtissues were incubated overnight with a custom-made collagen-specific CNAmCherry probe[16] at 24 and 96 h postrelease, fixed for 60 min using 10% formalin and stored in phosphate-buffered saline (PBS) at 4°C until imaging. Z-stack images were made using a confocal laser scanning microscope (TCS SP5X; Leica). The location of the Z-stack was always obtained from the center of the microtissue. The entire Z-stack, or until the detected fluorescent signal from the collagen probe was still sufficiently high to allow for quantification, was used for quantification of collagen orientation. Collagen fiber orientation was quantified using a previously developed custom-made fiber tracking algorithm,[17] based on the work of Frangi et al.[18] analyzing the individual images of each Z-stack. In brief, collagen orientation was determined via a multiscale approach in which the principal curvature directions from the eigenvalues and the eigenvectors of the Hessian matrix of the image (second order derivative) were calculated. For each image stack, a histogram containing fiber fraction per angle (ranging from 0° to 180° with a 2° interval) was obtained. Hereby, a matrix containing fiber fractions was obtained in which the number of rows represent the Z-stack (tissue) thickness and columns contain the 90 different angles. Subsequently, for each individual tissue, the average collagen fiber fraction for each angle was calculated throughout the complete Z-stack from the obtained matrix. Average fiber fractions for all tissues for the same protocol were used for bimodal fitting. To quantify the fiber distribution, the experimentally observed fractions were approximated by a bi-modal periodic normal probability distribution function using a nonlinear least-squares approximation algorithm:

$$\Phi_f(\gamma) = A_1 \exp\left[\frac{\cos[2(\gamma - \alpha_1)] + 1}{\beta_1}\right] + A_2 \exp\left[\frac{\cos[2(\gamma - \alpha_2)] + 1}{\beta_2}\right],$$

here, $\Phi_f(\gamma)$ is the fiber fraction as a function of the fiber angle γ. Variables α_1 and α_2 are the two main fiber angles and β_1 and β_2 represent the dispersity of the two fiber distributions. An angle of 90° is parallel to the long axis of the tissue. A_1 and A_2 are scaling factors for the total fiber fractions of the distributions. The quality of the bi-modal approximation is represented by the R^2 value. To compare collagen fiber distribution between groups, an order parameter was calculated for each measurement. The order parameter S was calculated as previously, adopted from a study by Hsu et al.[19]:

$$S = \int \Phi_f(\gamma)(\cos 2\gamma d\gamma).$$

Values for S range from −1 to 1, representing perfect alignment of collagen fibers to the longitudinal tissue orientation ($S = -1$), perfect perpendicular orientation of the collagen fibers to the longitudinal tissue direction ($S = 1$) and a random collagen fiber distribution ($S = 0$). At 24 h, a total of $N = 5$ LG/J and $N = 5$ C57BL/6J tissues were used for analyses. At 96 h, a total of $N = 6$ LG/J (of which $N = 2$ are pooled) and $N = 5$ C57BL/6J tissues were used for analyses.

2.6 | Immunohistochemistry

Microtissues were fixed, incubated in 30% sucrose overnight, embedded in Tissue-Tek and cut in sections (8 μm) using a cryotome and stored −20°C. Hereafter, the sections were thawed and hydrated in PBS and permeabilized with 1% triton-X followed by PBS washes. Afterward, sections were blocked with 2% goat serum and incubated with 5 ng/ml (dilution 1:100) Collagen type 1 Alpha 1 antibody (clone 3G3) (LS-B5932-50; LSBio) in 2% blocking buffer and incubated at 4°C overnight followed by PBS-tween and PBS washes. Sections were incubated with the secondary antibody, goat anti-mouse IgG3 Cross-Adsorbed, Alexa Fluor 488 (A-21151; Thermo Fisher Scientific) at dilution 1:500 and 4′,6-diamidino-2-phenylindole at dilution 1:500 in PBS for 60 min. Sections were washed with PBS-tween and PBS and mounted on glass slides with Mowiol (81381; Sigma-Aldrich). New production of mouse collagen (type I) at 96 h postrelease was visualized with a fluorescence microscope (Axiovert 200M; Zeiss) at ×40 magnification. Images were loaded into MATLAB and converted into 8-bit grayscale. After subtracting the background noise (all pixel intensities below 9 were discarded), all pixels with an intensity above 8 were counted and their total pixel intensity was calculated to semiquantify the amount of produced collagen. A total of $N = 6$ LG/J tissues and $N = 3$ C57BL/6J tissues were used for analyses. The mouse-specific collagen type I antibody in combination with the secondary antibody was confirmed to be specific for produced mouse collagen and did not cross-react with the rat collagen scaffold, established using the appropriate controls.

2.7 | Statistical analysis

Statistical analyses were performed using SPSS Statistics 25 for Windows (SPSS Inc.). All data are represented as mean and standard deviation. For surface area and waistcoat over time, comparison of the two mouse strains was made using two-way analysis of variance with Bonferroni-corrected independent t test posthoc testing at individual time points. For collagen outcome parameters at end time points, independent t test were used to test for differences between mouse strains. Differences were considered statistically different when $p < .05$. Before applying these tests, normality and homogeneity of variance was checked with a Shapiro-Wilkes test and Levene's test, respectively.
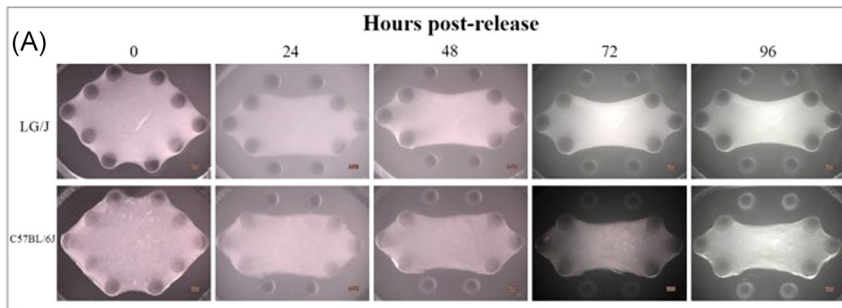
FIGURE 3 (A) Top-view contraction images at the different time points of LG/J and C57BL/6J microtissues. (B) Reduction in total surface area of the microtissues in hours postrelease [Color figure can be viewed at wileyonlinelibrary.com]
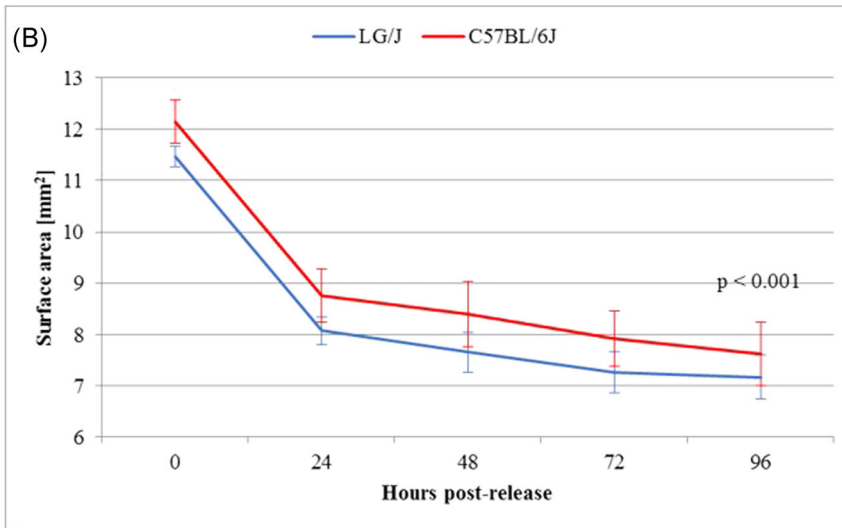
3 | RESULTS

3.1 | Surface area and waistcoat contraction

Top-view contraction images at the different time points of LG/J and C57BL/6J microtissues are shown in Figure 3. As expected, the greatest reduction in total surface area occurred directly after the microtissues were released from the perpendicular posts (Figure 3). In both groups,

the microtissues then continued to shrink in surface area at a constant similar rate over the next 3 days. Although the percentage of surface area contraction did not differ over 96 h postrelease, the LG/J AF microtissues were already significantly smaller immediately after release and remained smaller ($p < .001$) than those from the C57BL/6J mice during the entire period of observation.

In contrast to surface area, the rate of waistcoat of the microtissues followed a different pattern over time for both mouse strains.
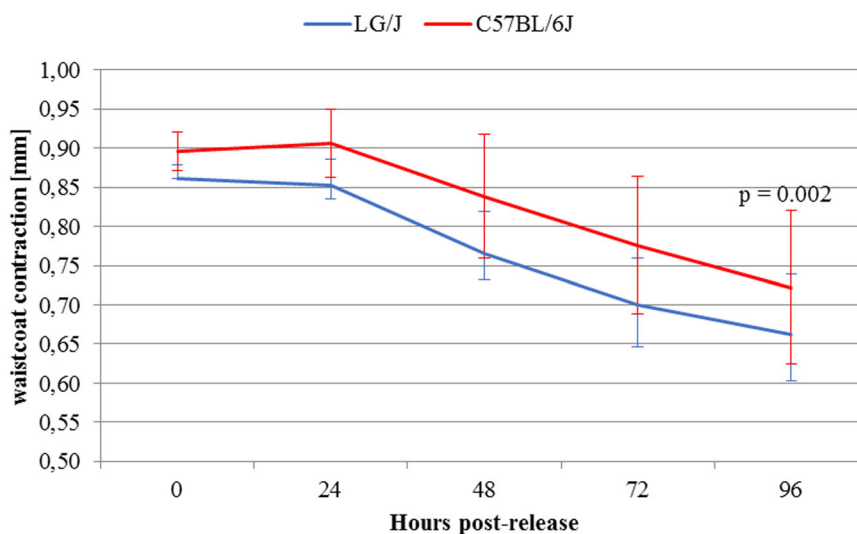
FIGURE 4 Waistcoat contraction of microtissues in hours postrelease [Color figure can be viewed at wileyonlinelibrary.com]

There was very little waistcoat contraction during the 1st day after release from the perpendicular posts, but substantial waistcoat contraction was observed over the following 3 days. Over this period, the rate was constant for both mouse strains (Figure 4). Immediately postrelease, there was more waistcoat contraction observed in microtissues from the LG/J AF mice than that from the C57BL/6J mice, and this remained significant throughout the 96-h observation period ($p = .002$).

3.2 | Collagen orientation

One day after release from the perpendicular posts, the collagen within the microtissues from both mouse strains appeared equally (randomly) oriented (Figure 5). In the microtissues with AF cells from C57BL/6J mice, this had not changed after 3 more days of culture. However, in case of cells from LG/J mice, collagen was observed to be more anisotropic in the longitudinal direction of the tissue (Figure 6). Quantification of collagen orientation showed no significant differences between the microtissues with AF cells of LG/J and C57BL/6J mice at 24 h. However, at 96 h, AF cells from LG/J mice were able to align the collagen better than those from C57BL/6J mice ($p < .001$; Figure 7).

3.3 | Collagen content

As the culture period of these microtissues was short, it was not expected that mouse cells produced a large amount of new collagen, detectable using quantitative techniques. Thus, we chose to stain for extra- and intracellular collagen with a mouse-specific collagen type I antibody.

Mostly intracellular collagen was noted. No differences in amount of collagen per nucleus count were seen between AF microtissues of LG/J and C57BL/6 J mice at the 96-h time point (Figure 8).

4 | DISCUSSION

The microtissue system was exploited to assess differences in collagen/tissue remodeling by AF cells between the C57BL/6J and LG/J mouse strain. This study demonstrates that AF cells of in-bred LG/J mice cultured in an in vitro microtissue assay system have more collagen remodeling/reorganization capacity than those from the C57BL/6J mice strain. Significant differences were detected for absolute tissue surface area, waistcoat contraction and collagen orientation. However, no difference was seen in newly synthesized collagen content of the microtissues. This could be due to the
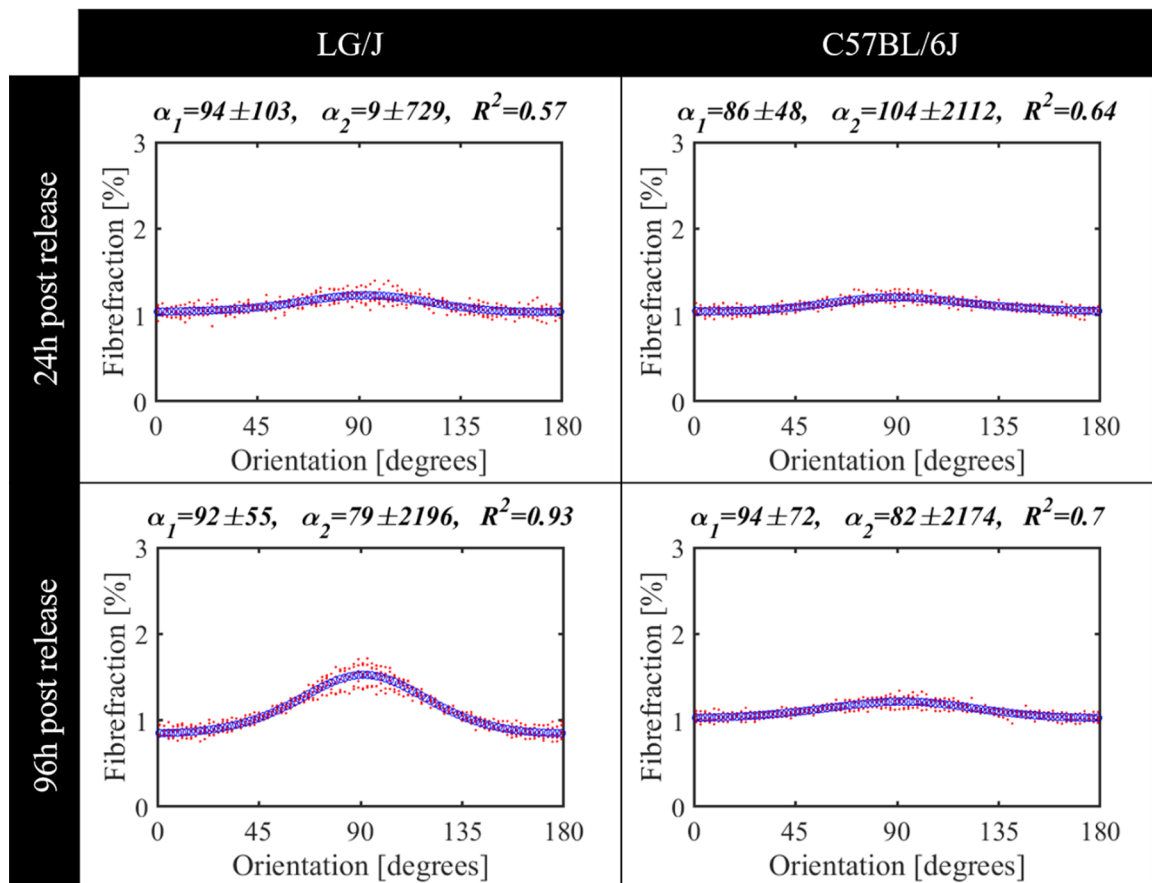
FIGURE 5 Orientation of AF fibers from both mouse strains 24 and 96 h postrelease. AF, annulus fibrosus [Color figure can be viewed at wileyonlinelibrary.com]
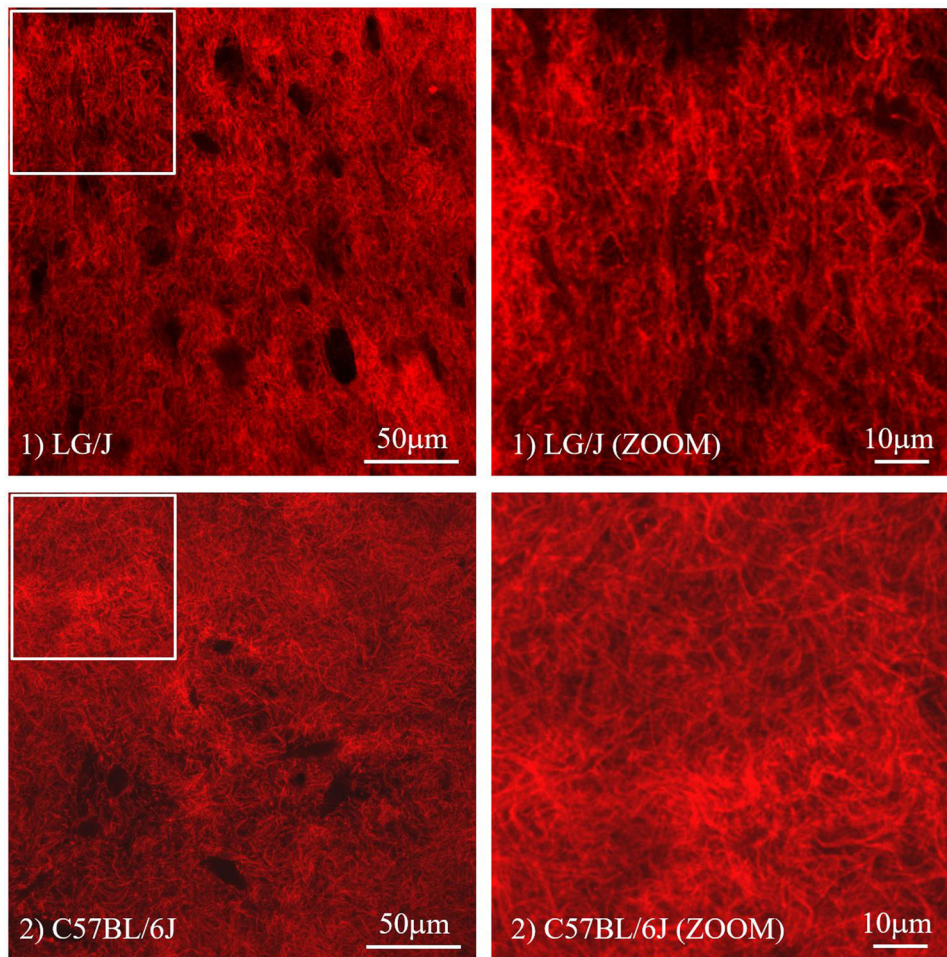
FIGURE 6 Confocal microscope image of CNAmCherry stained tissues 96 h postrelease of (1) AF LG/J and (2) C57BL/6J [Color figure can be viewed at wileyonlinelibrary.com]

relatively short culture period that was used in this experiment, or that these cells, suspended in a hydrogel mixture of collagen are not sufficiently driven to produce collagen.

The microtissue system used in our experiment, was originally designed as an in vitro model to study aspects of the tendon scarring process and the cellular response in tissue remodeling/reorganization[14] and has also been used for fibroblasts.[20] Healthy tendon contains high amounts of collagen type I and low amounts of collagen type III.[21] Like tendon, the AF also contains collagen,[22] consisting mostly of collagen types I and II, where type I is mostly found in the AF.[23] Using this in vitro model, we show that LG/J AF cells are able to more extensively reorganize the collagen network within the microtissue compared to C57BL/6J AF cells.

In our experiment we used in-bred strains of mice with known differences in their connective tissue healing capacity. The LG/J mice strain (a parental line of MRL/MpJ) have shown to have similar if not better healing capabilities of articular cartilage and ear wound healing than MRL/MpJ, the original strain identified with wound regeneration capabilities. The MRL/MpJ is a "fast healer" for numerous types of injuries such as skin and cardiac wound and nerve injuries. More recently, The LG/J and MRL/MpJ have also shown to display quicker

irreversible disc wedging and this could be due to the fact that MRL mice are able to more quickly and extensively remodel their AF tissue.[12] The extracellular matrix of articular cartilage consists of proteoglycans and collagens (type II, VI, IX, X, and X1).[11,24,25] This suggests that a common factor, such as collagens in both types of tissues (AF and cartilage), and remodeling of these collagens could be a driving factor behind improved regeneration/remodeling.

The MRL/MpJ mice strain and the parental LG/J strain have demonstrated superior regenerative capacities of body tissues, such as ear wound healing and cartilage repair.[11] Many mechanisms have been identified that could potentially explain these regenerative properties, including increased proliferation and migration of cells,[26,27] increased tenascin expression[28] and increased extracellular matrix production and angiogenesis.[26] Additionally, molecular mechanisms showing regenerative potential in MRL/MpJ have also emerged. The healing potential of the retina in MRL/MpJ was linked to elevated expression of matrix metalloproteinases,[29] and in regeneration of amputated digits, a number of keratin genes were differentially expressed between MRL/MpJ and C57BL/6 mice.[30] While several biological processes have been suggested to cause elevated healing capabilities in
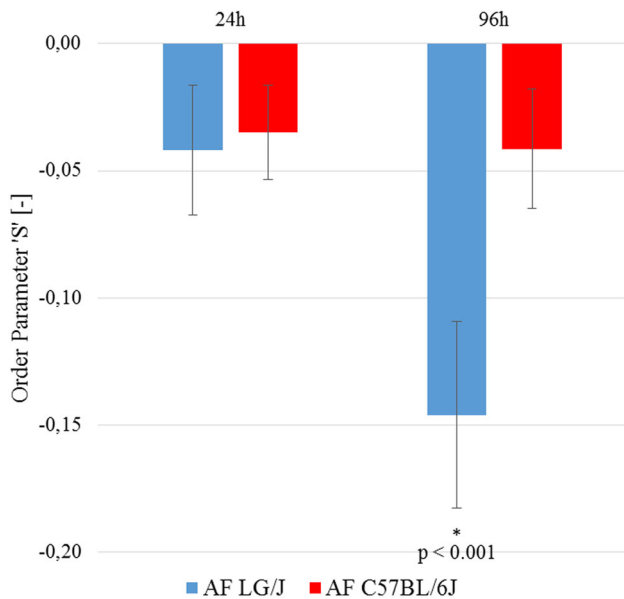
FIGURE 7 Quantification of collagen orientation showed no significant differences between the microtissues with AF cells of LG/J and C57BL/6J mice at 24 h. However, at 96 h, AF cells from LG/J mice were able to align the collagen better than those from C57BL/6J mice. AF, annulus fibrosus [Color figure can be viewed at wileyonlinelibrary.com]

these mice, the data is insufficient to demonstrate conclusively why these mice regenerate better.[11]

As mentioned earlier, the IVD may be an important factor in the onset and progression of scoliosis and irreversible changes in the IVD, in particular the AF, may support or enhance scoliosis curve progression. We hypothesized that potential curve progression differences could be distinguishable by measuring collagen network adaptation potential of an individual's AF cells. As an initial exploration of this hypothesis, we determined whether AF cells of in-bred LG/J and C57BL/6J mice (normal healers) strains show a difference in collagen remodeling capacity in an in vitro microtissue assay system. The result of our experiments shows that there are differences in collagen remodeling between two strains of mice. Even though the mice strains

are genetically different, our results could imply that it is possible that similar cell types act differently under remodeling circumstances (because of still unknown underlying biological processes).

There are some limitations to this study. Because of the poor expansion of the AF cells, it was not possible to have all microtissues with cells from individual mice. Some samples consisted of pooled cells mostly from one donor, supplemented with cells from other donors. As such the samples are not strictly biologically independent. However, the proportion of supplementary cells were minor and there was no difference in the results when the samples were divided into two subgroups and compared (pooled vs. nonpooled). Due to technical difficulties, some outcomes had a smaller number of replicates than planned although it was sufficient to detect significant difference. The short amount of time in culture of the microtissues was another limitation. However, the time points and cell densities were selected to capture direct adaptation of the collagen by the cultured cells as shown in previous experiments.[31–33] With the current set-up, a longer culture period was not possible because the amount of AF cells in the microtissue literally pulled the tissues off the posts due to the increasing tension, breaking the tissues. Even with the short times used in this study, this was still not avoidable with all microtissues. Even though the same cell density was used to create the microtissues, over the 6 day culture, cell density may have become different for both mouse strains. Such differences in cell number could have accounted for differences in collagen and tissue adaptation. A preliminary calculation of the amount of nuclei present in our immunohistogical slices, did show a higher cell density for the LG/J tissues, but this was not significantly different from the C57. We do however realize that this quantification is not highly reliable. Thus, if cell density were similar, the observed differences are highly likely to be related to phenotypic differences. This could have been confirmed with PCR or western blot analysis, but there were unfortunately not enough tissues for these additional assays. The experiments are performed with cells from only in-bred strains of mice and it is still far from translation to testing for cells from individual humans, it does demonstrate the possibilities that macroscopic behavior at the disc organ level may be detected by examining the behavior of cells sampled from the tissue.

FIGURE 8 Fluorescence microscope image (×40 magnification) of newly produced mouse collagen type I at 96 h postrelease of (1) AF LG/J and (2) AF C57BL/6J tissues [Color figure can be viewed at wileyonlinelibrary.com]
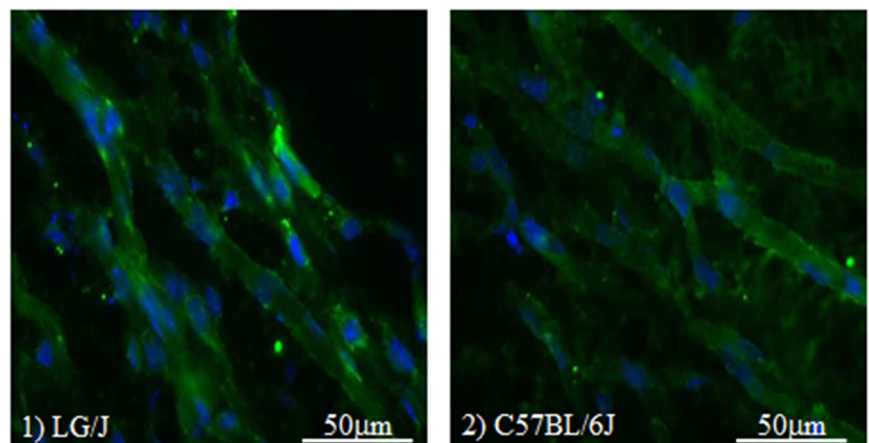
In conclusion, AF cells of in-bred LG/J and C57BL/6J mice strains show a difference in collagen remodeling/reorganization capacity in an in vitro microtissue assay system.

AUTHOR CONTRIBUTIONS

Substantial contribution to research design: Isabel N. Tromp, Jasper Foolen, Danny Chan, Moyo C. Kruyt, Laura B. Creemers, Rene M. Castelein, and Keita Ito. *Acquisition of data*: Isabel N. Tromp, Jasper Foolen, Marina van Doeselaar, and Ying Zhang. *Analysis and interpretation*: Isabel N. Tromp, Jasper Foolen, Marina van Doeselaar, Ying Zhang, and Keita Ito. *Drafting the article*: Isabel N. Tromp. *Revising it critically*: Jasper Foolen, Marina van Doeselaar, Ying Zhang, Danny Chan, Moyo C. Kruyt, Laura B. Creemers, Rene M. Castelein, and Keita Ito. *Approval of the submitted and final version*: Isabel N. Tromp, Jasper Foolen, Marina van Doeselaar, Ying Zhang, Danny Chan, Moyo C. Kruyt, Laura B. Creemers, Rene M. Castelein, and Keita Ito.

ORCID

Keita Ito https://orcid.org/0000-0002-7372-4072

REFERENCES

1. Kouwenhoven J-WM, Castelein RM. The pathogenesis of adolescent idiopathic scoliosis: review of the literature. *Spine (Phila Pa 1976)*. 2008;33(26):2898-2908.
2. Cheng JC, Castelein RM, Chu WC, et al. Adolescent idiopathic scoliosis. *Nat Rev Dis Prim*. 2015;1:15030.
3. Will RE, Stokes IA, Qiu X, Walker MR, Sanders JO. Cobb angle progression in adolescent scoliosis begins at the intervertebral disc. *Spine (Phila Pa 1976)*. 2009;34(25):2782-2786.
4. Schlösser TPC, van Stralen M, Brink RC, et al. Three-dimensional characterization of torsion and asymmetry of the intervertebral discs versus vertebral bodies in adolescent idiopathic scoliosis. *Spine (Phila Pa 1976)*. 2014;39(19):E1159-E1166.
5. Yu J, Fairbank JCT, Roberts S, Urban JPG. The elastic fiber network of the anulus fibrosus of the normal and scoliotic human intervertebral disc. *Spine (Phila Pa 1976)*. 2005;30(16):1815-1820.
6. Brickley-Parsons D, Glimcher MJ. Is the chemistry of collagen in intervertebral discs an expression of Wolff's Law? A study of the human lumbar spine. *Spine (Phila Pa 1976)*. 1984;9(2):148-163.
7. Bushell GR, Ghosh P, Taylor TK, Sutherland JM. The collagen of the intervertebral disc in adolescent idiopathic scoliosis. *J Bone Joint Surg Br*. 1979;61-B(4):501-508.
8. Duance VC, Crean JKG, Sims TJ, et al. Changes in collagen cross-linking in degenerative disc disease and scoliosis. *Spine (Phila Pa 1976)*. 1998;23(23):2545-2551.
9. Langlais T, Vergari C, Pietton R, Dubousset J, Skalli W, Vialle R. Shear-wave elastography can evaluate annulus fibrosus alteration in adolescent scoliosis. *Eur Radiol*. 2018;28:1-8.
10. Sakai D, Nishimura K, Tanaka M, et al. Migration of bone marrow-derived cells for endogenous repair in a new tail-looping disc degeneration model in the mouse: a pilot study. *Spine J*. 2015;15(6):1356-1365.
11. Rai MF, Sandell LJ. Regeneration of articular cartilage in healer and non-healer mice. *Matrix Biol*. 2014;39:50-55.
12. Zhang Y 2017. Intervertebral disc maintenance and repair potential in mice (PhD Thesis).
13. Zhang Y, Xiong C, Kudelko M, et al. Early onset of disc degeneration in SM/J mice is associated with changes in ion transport systems and fibrotic events. *Matrix Biol*. 2018;70:123-139.
14. Foolen J, Wunderli SL, Loerakker S, Snedeker JG. Tissue alignment enhances remodeling potential of tendon-derived cells—lessons from a novel microtissue model of tendon scarring. *Matrix Biol*. 2018;65:14-29.
15. Schindelin J, Arganda-Carreras I, Frise E, et al. Fiji: an open-source platform for biological-image analysis. *Nat Methods*. 2012;9(7):676-682.
16. Aper SJA, Van Spreeuwel ACC, Van Turnhout MC, et al. Colorful protein-based fluorescent probes for collagen imaging. *PLOS One*. 2014;9(12):1-21.
17. Foolen J, Deshpande VS, Kanters FMW, Baaijens FPT. The influence of matrix integrity on stress-fiber remodeling in 3D. *Biomaterials*. 2012;33(30):7508-7518.
18. Frangi AF, Niessen WJ, Vincken KL, Viergever MA. MUltiscale Vessel Enhancement Filtering. In: Wells WM, Colchester A, Delp S, eds. *Medical Image Computing and Computer-Assisted Intervention—MICCAI'98*. Berlin Heidelberg: Springer; 1998:130-137.
19. Hsu HJ, Lee CF, Locke A, Vanderzyl SQ, Kaunas R. Stretch-induced stress fiber remodeling and the activations of JNK and ERK depend on mechanical strain rate, but not FAK. *PLOS One*. 2010;5(8): e12470.
20. van Vijven M, van Groningen B, Kimenai JN, et al. Identifying potential patient-specific predictors for anterior cruciate ligament reconstruction outcome—a diagnostic in vitro tissue remodeling platform. *J Exp Orthop*. 2020;7(1):48.
21. Williams IF, Heaton A, McCullagh KG. Cell morphology and collagen types in equine tendon scar. *Res Vet Sci*. 1980;28(3):302-310.
22. Hormel SE, Eyre DR. Collagen in the ageing human intervertebral disc: an increase in covalently bound fluorophores and chromophores. *Biochim Biophys Acta*. 1991;1078(2):243-250.
23. Eyre DR, Muir H. Collagen polymorphism: two molecular species in pig intervertebral disc. *FEBS Lett*. 1974;42(2):192-196.
24. Poole AR, Kojima T, Yasuda T, et al. Composition and structure of articular cartilage: a template for tissue repair. *Clin Orthop Relat Res*. 2001;391:S26-S33.
25. Poole CA, Glant TT, Schofield JR. Chondrons from articular cartilage. (IV) Immunolocalization of proteoglycan epitopes in isolated canine tibial chondrons. *J Histochem Cytochem*. 1991;39(9):1175-1187.
26. Clark LD, Clark RK, Heber-Katz E. A new murine model for mammalian wound repair and regeneration we describe herein a mouse model of wound repair. *Clin Immunol Immunopathol*. 1998;88(1):35-45.
27. Leferovich JM, Bedelbaeva K, Samulewicz S, et al. Heart regeneration in adult MRL mice. *Proc Natl Acad Sci USA*. 2001;98(17):9830-9835.
28. Haris Naseem R, Meeson AP, Michael DiMaio J, et al. Reparative myocardial mechanisms in adult C57BL/6 and MRL mice following injury. *Physiol Genomics*. 2007;30(1):44-52.
29. Tucker B, Klassen H, Yang L, Chen DF, Young MJ. Elevated MMP expression in the MRL mouse retina creates a permissive environment for retinal regeneration. *Invest Ophthalmol Vis Sci*. 2008;49(4):1686-1695.
30. Cheng C-H, Leferovich J, Zhang X-M, et al. Keratin gene expression profiles after digit amputation in C57BL/6 vs. regenerative MRL mice imply an early regenerative keratinocyte activated-like state. *Physiol Genomics*. 2013;45(11):409-421.
31. Foolen J, Shiu JY, Mitsi M, Zhang Y, Chen CS, Vogel V. Full-length fibronectin drives fibroblast accumulation at the surface of collagen microtissues during cell-induced tissue morphogenesis. *PLOS One*. 2016;11(8):1-24.

32. Foolen J, Janssen-Van Den Broek MWJT, Baaijens FPT. Synergy between Rho signaling and matrix density in cyclic stretch-induced stress fiber organization. *Acta Biomater*. 2014;10(5):1876-1885.

33. Foolen J., Deshpande V., Baaijens F. 2012. Stress-fiber remodeling in 3D: "Contact guidance vs stretch avoidance." American Society of Mechanical Engineers 2012 Summer Bioengineering Conference. pp. 1295–1296.